

# Lateral current density fronts in asymmetric double-barrier resonant-tunneling structures

Pavel Rodin\* and Eckehard Schöll

*Institut für Theoretische Physik, Technische Universität Berlin,  
Hardenbergstrasse 36, D-10623, Berlin, Germany*

(October 30, 2018)

We present a theoretical analysis and numerical simulations of lateral current density fronts in bistable resonant-tunneling diodes with Z-shaped current-voltage characteristics. The bistability is due to the charge accumulation in the quantum well of the double-barrier structure. We focus on asymmetric structures in the regime of sequential incoherent tunneling and study the dependence of the bistability range, the front velocity and the front width on the structure parameters. We propose a sectional design of a structure that is suitable for experimental observation of front propagation and discuss potential problems of such measurements in view of our theoretical findings. We point out the possibility to use sectional resonant-tunneling structures as controllable three-terminal switches.

PACS 05.70.Ln,72.20.Ht,85.30.-z

## I. INTRODUCTION

Charge accumulation in the well of a double-barrier resonant tunneling (DBRT) structure leads to electrostatic feedback that increases the energy of the quasi-bound state with respect to the emitter, thus making resonant tunneling possible for higher applied voltages<sup>1</sup>. This may result in bistability when the high current density and low current density states coexist in a certain range of the applied voltage. The current-voltage characteristic becomes Z-shaped instead of the conventional N-shape<sup>1,2</sup>. It has been pointed out that the bistability provides a basis for formation of lateral current density patterns like traveling current density fronts<sup>3-6</sup>. Once triggered, such a front leads to switching of the structure between the on- and off-state, depending on the applied voltage<sup>4-7</sup>. Front propagation in the DBRT provides a unique example of nonlinear pattern formation in a system with quantum transport. In the context of the DBRT studies, it represents a novel switching process (*trigger front*) which is spatially inhomogeneous and is likely to determine the general properties of switching dynamics in large-area DBRT structures.

Recent theoretical work<sup>4-9</sup> has essentially focused on the *qualitative* behavior of current density fronts, whereas the possibility of their experimental observation crucially depends on *quantitative* parameters, first of all on the front propagation velocity and the front width. This is due to the limits of temporal resolution and finite lateral dimensions of DBRT structures. In this article we aim to bridge this gap and present the results of numerical simulations of front dynamics in asymmetric DBRT structures that provide a wide range of bistability and thus are favorable for experimental observation. We also discuss the specific design of DBRT structures that are suitable for such experiments.

## II. MODEL OF THE DBRT STRUCTURE

The bistability of a DBRT structure occurs due to the charge accumulation in the quantum well<sup>1,2</sup>. As a result of the electrostatic feedback the potential of the bottom of the well  $\Phi$  depends not only on the applied voltage  $u$ , but also on the built-up electron concentration  $n$  (Fig.1). For structures with narrow well and thick barriers the  $\Phi(u, n)$  dependence can be calculated by representing electrons in the well as a sheet charge of negligible width<sup>8</sup>:

$$\Phi(u, n) = -\frac{b_1}{d}u + \frac{b_1 b_2}{d} \frac{en(x, y)}{\epsilon \epsilon_0}, \quad d = b_1 + b_2. \quad (1)$$

Here  $u < 0$  is the applied voltage,  $e < 0$  is the electron charge,  $\epsilon$  and  $\epsilon_0$  are the relative and absolute permittivities of the material, respectively. The effective widths of the emitter-well barrier  $b_1$  and the well-collector barrier  $b_2$  include the half-width of the well, and  $b_2$  also includes the width of the depleted collector layer (Fig.1)<sup>13</sup>. Eqn.(1) is also applicable in the case when the built-up concentration is inhomogeneously distributed in the transverse  $(x, y)$ -plane, provided that the transverse variations of  $n(x, y, t)$  are smooth in the sense that their characteristic length is much larger than the effective thickness of the structure  $d$ . Below we will show that this condition is indeed met for current density fronts.

In the regime of sequential tunneling the DBRT structure can be described by the continuity equation for the electron density per unit area in the well  $n(x, y, t)$ <sup>3,4,6,7,9</sup>

$$\frac{\partial n}{\partial t} + \frac{1}{e} \nabla_{\perp} \mathbf{J}_{\perp} = \frac{1}{e} (J_{ew} - J_{wc}), \quad (2)$$

$$\nabla_{\perp} \equiv \mathbf{e}_x \frac{\partial}{\partial x} + \mathbf{e}_y \frac{\partial}{\partial y},$$

where  $J_{ew}(x, y)$  and  $J_{wc}(x, y)$  are local densities (per unit area) of the emitter-well and the well-collector currents,

respectively,  $\mathbf{J}_\perp$  is the density (per unit length) of the transverse current in the well.

The transverse redistribution of charge in the well is treated semiclassically in the drift-diffusion approximation according to Ref. 8. The drift component of  $\mathbf{J}_\perp$  is proportional to the lateral electrical field  $\mathcal{E}_\perp = -\nabla_\perp \Phi$ . Eq.(1) yields  $\mathcal{E}_\perp \sim \nabla_\perp n$ , and hence the drift current, similar to the diffusive current, turns out to be proportional to the gradient of the built-up electron concentration. This allow us to represent the transverse current density in the well in terms of an effective concentration-dependent diffusion coefficient  $D(n)$ <sup>8</sup>:

$$\mathbf{J}_\perp = -eD(n)\nabla_\perp n, \quad (3)$$

$$D(n) = \frac{|e|\mu n}{4\epsilon\epsilon_0} \left( \frac{4b_1b_2}{d} + \frac{r_B}{1 - \exp[-n/(\rho_0kT_W)]} \right).$$

Here  $\mu$  is electron mobility in the well,  $r_B = (4\pi\epsilon\epsilon_0\hbar^2)/(e^2m)$  is Bohr radius in the semiconductor material,  $\rho_0 = m/(\pi\hbar^2)$  is the 2D density of states,  $m$  is the effective electron mass and  $k$  is Boltzmann's constant. The derivation of Eq.(3) assumes a Fermi distribution in the well<sup>8</sup>. The electron temperature  $T_W$  in the well can be different from the substrate temperature  $T$ . In the following we assume a substrate temperature  $T = 4$  K.

The emitter-well and well-collector current densities are modelled by simple approximate formulas<sup>7,9,10</sup>

$$J_{ew} = \frac{e\Gamma_L}{\hbar} [\rho_0\Delta - n] \times \frac{\arctan(2\Delta/\Gamma_W) - \arctan(2\Omega/\Gamma_W)}{\pi}, \quad (4)$$

$$J_{wc} = \frac{e\Gamma_R}{\hbar} n, \quad (5)$$

where

$$\Delta(n, u) \equiv E_e^F - E_W - e\Phi, \quad \Omega(n, u) \equiv -E_W - e\Phi \quad (6)$$

denote the energy of the quasibound state with respect to the Fermi level and the bottom of the conduction band in the emitter, respectively,  $E_e^F$  is the Fermi energy in the emitter,  $E_W > E_e^F$  is the energy of the quasibound state with respect to the bottom of the well,  $\Gamma_L$  and  $\Gamma_R$  are the energy broadenings associated with the emitter-well and the well-collector barriers, respectively,  $\Gamma_W = \Gamma_L + \Gamma_R + \Gamma_{scatt}$  is the total broadening of the quasi-bound state resulting from the escape *via* emitter-well barrier, well-collector barrier and scattering in the well, respectively. The broadening of the quasibound state is characterized by a Lorentzian spectral function. The assumption of sequential tunneling implies that  $\Gamma_L, \Gamma_R < \Gamma_{scatt}$ . Similar models for vertical transport have also been used in Refs. 6, 11.

Eqn.(4) has a transparent physical meaning:  $\Gamma_L/\hbar$  is the tunneling rate between the emitter and the well;  $[\rho_0\Delta - n]$  is the difference between the number of transverse tunneling modes available for the given position of the quasibound state<sup>12</sup> and the number of occupied

states in the well; the last factor accounts for smooth decrease of current near the resonance breaking points  $\Delta = 0$  and  $\Omega = 0$ . Eqn.(5) describes the one-way tunneling from the well to the collector with a rate  $\Gamma_R/\hbar$ . In the stationary state the current density  $J$  is proportional to the electron concentration  $n$  stored in the well. Formal derivation of this transport model<sup>7,9</sup> is based on the following essential assumptions:

(i) barriers are high in the sense that the matrix element of the emitter-well and well-collector transitions do not depend on the vertical (in  $z$ -direction) electron momentum, hence the barriers are fully characterized by constant transparencies  $\Gamma_{L,R}$ ;

(ii) the temperature of the substrate  $T$  and the electron temperature of the well  $T_W$  are small compared to  $E_e^F$  and  $\Gamma_W$ ;

(iii) the Fermi level in the collector is lower than the bottom of the well.

Combining (1)–(5) and taking into account only one transverse dimension, we obtain the following nonlinear parabolic equation for the built-up electron charge

$$\frac{\partial n}{\partial t} = \frac{\partial}{\partial x} \left( D(n) \frac{\partial n}{\partial x} \right) + f(n, u), \quad (7)$$

$$f(n, u) = \frac{1}{e} (J_{ew}(u, n) - J_{wc}(n)).$$

In the stationary state  $J = J_{ew} = J_{wc}$ , and the local current-voltage characteristic  $J(u) = J(u, n(u))$  is determined by the stationary  $n(u)$ -dependence together with Eqns.(4),(5). The  $n(u)$ -dependence, in turn, follows from the steady-state condition  $f(n, u) = 0$ . The  $J(u)$  characteristic is bistable for sufficiently small broadening of the quasi-bound state  $\Gamma_W$ . A typical example of such Z-shaped characteristics is shown in Fig.2.

We use the following set of material and structure parameters:  $\epsilon = 12$  and  $m = 0.067 m_0$  (for GaAs), where  $m_0$  is the free electron mass;  $E_e^F = 10$  meV,  $\mu = 10^5$  cm<sup>2</sup>/Vs,  $E_W = 40$  meV,  $T = 4$  K. The effective width of the emitter-well barrier is taken as  $b_1 = 10$  nm. The effective width of the second barrier  $b_2$  includes the width of the depletion layer in the collector  $l_d \sim (\epsilon\epsilon_0 u)/(eN_D d)$  (see Fig.1), which lies in the interval 10...100 nm for the typical doping level  $N_D = 10^{17}$  cm<sup>-3</sup> in the collector<sup>13</sup>.

The dependence of the transparencies  $\Gamma_L$  and  $\Gamma_R$  on the actual barrier widths can be evaluated by solving the one-dimensional Schrödinger equation<sup>14</sup>. Compact formulas for the transparencies of GaAs/AlGaAs barriers are given in Ref. 15. Typical values are  $\Gamma_{L,R} \sim 0.1...1$  meV for barrier widths of the order of 10 nm<sup>15</sup>. The corresponding tunneling time is  $\tau_T \sim 0.06...0.6$  ps. The parameter  $\Gamma_{scatt}$  can be estimated on the basis of the electron mobility in the quantum well. Typical mobility values  $\mu \sim 10^4...10^5$  cm<sup>2</sup>/Vs yield  $\Gamma_{scatt} \sim e\hbar/m\mu \sim 0.1...1$  meV<sup>16,17</sup>. The corresponding momentum relaxation time  $\tau_m$  is of the order of 1 ps or less. Below we assume the total broadening of the quasibound

state to be  $\Gamma_W = 1...2$  meV, and take into account that  $\Gamma_L, \Gamma_R < \Gamma_W$ . After tunneling from the emitter to the quantum well the transverse kinetic energy of an electron is transferred to the lattice. The temperature of the electron gas in the well depends on the relation between the energy relaxation time  $\tau_e$  and the tunneling time  $\tau_T$ <sup>18</sup>. The limit cases  $\tau_e \ll \tau_T$  and  $\tau_e \gg \tau_T$  correspond to a cold ( $T_W \approx T$ ) and hot ( $T_W > T$ ) electron gas, respectively. Since for resonant tunneling conditions the transverse kinetic energy is limited by  $E_e^F$ , the upper bound for the electron temperature is given by  $T_W = E_e^F/k \approx 100$  K. Below we consider the whole range of relevant temperatures  $T < T_W < E_e^F/k$  and find that the effect of electron heating on the front dynamics is negligible.

### III. RANGE OF BISTABILITY

We shall start with two simple analytical estimates for the range of bistability  $\Delta u \equiv |u_{th} - u_h|$ , where  $u_h$  and  $u_{th}$  are the left and right turning points of the Z-shaped current-voltage characteristic that correspond to the holding and threshold voltages, respectively (see Fig.2). In the limit  $\Gamma_W \ll E_e^F$  the current-voltage characteristic becomes piecewise linear. Then the ultimate upper bound for the bistability range  $\Delta u$  immediately follows from Eqns.(4),(5) and the condition  $J_{ew} = J_{wc}$  (see also (A3) in the Appendix):

$$\Delta u = \frac{1}{|e|} \frac{4\Gamma_L}{\Gamma_L + \Gamma_R} \frac{b_2}{r_B} E_e^F. \quad (8)$$

Eq.(8) indicates that low transparency  $\Gamma_R$  and large effective thickness  $b_2$  of the well-collector barrier are favorable for bistability. (Note that with increasing  $d$  the intrinsic capacitance of the well becomes smaller, enhancing the electrostatic feedback from the built-up electron charge.)

For finite broadening of the quasibound state  $\Gamma_W$  the bistability range shrinks or even disappears. This effect can be evaluated analytically by using a square-shaped spectral function

$$A_W(E, \mathbf{k}) = \frac{1}{\Gamma_W} (\Theta(E - E_k - E_W - e\Phi_W + \Gamma_W/2) - \Theta(E - E_k - E_W - e\Phi_W - \Gamma_W/2)), \quad (9)$$

where  $\Theta$  is the Heaviside function, instead of the Lorentzian spectral function

$$A_W(E, \mathbf{k}) = \frac{\Gamma_W}{[(E - E_k - E_W - e\Phi_W)^2 + \Gamma_W^2/4]}, \quad (10)$$

that has been used to derive Eqns.(4),(5). (Here  $\mathbf{k}$  is the transverse electron momentum and  $E_k$  is the corresponding kinetic energy.) This substitution yields

$$\Delta u \approx \frac{1}{|e|} \left[ \frac{4\Gamma_L}{\Gamma_L + \Gamma_R} \frac{b_2}{r_B} \left( E_e^F - \frac{\Gamma_W}{2} \right) - \frac{d}{b_1} \Gamma_W \right]. \quad (11)$$

According to (11), the effect of geometrical asymmetry  $b_1 \neq b_2$  is not monotonic: for fixed total width  $d = \text{const}$  there is an optimal ratio

$$\frac{b_1}{d} = \sqrt{\frac{\Gamma_L + \Gamma_R}{2\Gamma_L} \frac{r_B}{d} \frac{\Gamma_W}{2E_e^F - \Gamma_W}}. \quad (12)$$

Eqn.(11), along with Eqn.(8), predicts that  $\Delta u$  monotonically increases with decrease of the  $\Gamma_R/\Gamma_L$  ratio. In contrast to this conclusion, the ranges of bistability calculated numerically for the full model (4),(5) (see Fig.3) show that there is an optimal ratio  $\Gamma_R/\Gamma_L$ , roughly  $\Gamma_R/\Gamma_L \approx 0.2$ , that corresponds to the widest bistability range. When  $\Gamma_R$  is too small, the bistability vanishes due to the relative increase of current density in the off-state. Eqn.(11) does not catch this effect because the oversimplified spectral function (9) inadequately describes the low-branch of the current-voltage characteristic<sup>19</sup>.

### IV. STATIONARY PROPAGATING FRONTS

*General properties.* Stationary moving fronts correspond to self-similar solutions of Eqn.(7)  $n(x, t) = n(x - vt)$  satisfying the boundary conditions  $n(-\infty) = n_{on}$ ,  $n(+\infty) = n_{off}$ , where  $n_{on}$  and  $n_{off}$  are the electron concentrations in the well in the on- and off-states, respectively. Such solutions give a good approximation for fronts in a finite system with lateral size  $L$  much larger than the front width  $W$ , regardless of the actual boundary conditions for built-up concentrations at the lateral edges of the DBRT. A positive velocity  $v > 0$  corresponds to propagation of the on-state into the off-state (hot front), a negative velocity corresponds to propagation of the off-state into the on-state (cold front); this triggers switching between the two states. In the co-moving frame  $\xi = x - vt$  Eqn.(7) becomes an ordinary differential equation

$$\frac{d}{d\xi} \left( D(n) \frac{dn}{d\xi} \right) + v \frac{dn}{d\xi} + f(n, u) = 0. \quad (13)$$

Multiplying by  $D(n)dn/d\xi$  and integrating over  $\int_{-\infty}^{+\infty} d\xi$  yields<sup>20</sup>

$$v = \frac{\int_{n_{off}}^{n_{on}} f(n, u) D(n) dn}{\int_{-\infty}^{\infty} (dn/d\xi)^2 D(n) d\xi}. \quad (14)$$

The direction of front propagation is determined by the sign of the numerator in Eq.(14), and hence by the applied voltage  $u$ . The equal areas rule  $\int_{n_{off}}^{n_{on}} f(n, u_{co}) D(n) dn$  corresponds to  $v = 0$  and specifies the voltage  $u_{co}$  at which a stationary current density front exists.

*Formula for the front velocity.* In the limit case of small broadening of the quasibound state  $\Gamma_W \ll E_e^F$  equation

(13) can be integrated analytically, if we additionally assume  $D(n) = D_0 = \text{const}$  (see Appendix). This leads to the following approximate  $v(u)$ -dependence

$$v = \sqrt{\frac{\Gamma_L D_0}{\hbar}} \frac{(1 + \sqrt{\alpha_{RL} A})^2}{2A} \frac{r_B}{b_2} \frac{|e|(u - u_{co})}{E_e^F}, \quad (15)$$

where

$$\lambda \equiv \frac{4b_1 b_2}{dr_B}, \quad \alpha_{RL} \equiv \frac{\Gamma_R}{\Gamma_L}, \quad A \equiv \sqrt{\lambda + \alpha_{RL} + 1} + \sqrt{\alpha_{RL}}$$

and  $u_{co}$  is determined by (A8). Generally, Eqn.(15) is applicable to slow fronts when  $|e|(u - u_{co}) \ll E_e^F$ .

The diffusion coefficient  $D_0$  can be estimated on the basis of Eqn.(3), assuming drift-dominated transport in the well and choosing an average concentration  $\langle n \rangle$  in the front wall

$$D_0 \approx \frac{|e|\mu b_1 b_2}{\epsilon \epsilon_0 d} \langle n \rangle = \frac{\mu \lambda}{|e|\rho_o} \langle n \rangle, \quad (16)$$

$$\langle n \rangle = \frac{n_{on}(u_{co}) + n_{off}(u_{co})}{2},$$

where  $n_{on}(u_{co})$  and  $n_{off}(u_{co})$  are the electron concentrations in the well for on- and off-states at  $u = u_{co}$ , respectively. (We note that the assumption of drift-dominated transport is supported by the numerical results presented below.) Using (A4) and (A8), we substitute (16) into (15) and get

$$v = \sqrt{\frac{\mu \Gamma_L E_e^F}{e \hbar}} \times \sqrt{\frac{(1 + \sqrt{\alpha_{RL} A})^3 (1 + \lambda + \sqrt{\alpha_{RL} A})}{\lambda (\lambda + \alpha_{RL} + 1) A^2}} \times \frac{b_1}{d} \frac{|e|(u - u_{co})}{E_e^F}. \quad (17)$$

According to (8) the width of the bistability range  $\Delta u$  is of order of  $E_e^F$ , and the second factor in (18) is of the order of unity for realistic structure parameters. Hence the order of magnitude value of the front velocity is given by

$$v \sim \sqrt{\frac{\mu \Gamma_L E_e^F}{e \hbar}}. \quad (18)$$

We get  $v \sim 10^7$  cm/s for  $E_e^F = 10$  meV,  $\Gamma_L = 1$  meV and  $\mu = 10^5$  cm<sup>2</sup>/Vs.

*Numerical results.* Numerical results for the front velocity  $v(u)$  and front width  $W(u)$  are summarized in Fig.4. It follows from Eqn.(7) that these quantities scale as

$$v \sim \sqrt{Df} \quad \text{and} \quad W \sim \sqrt{\frac{D}{f}}, \quad (19)$$

respectively. The scaling rules (19) allow one to extend the numerical results to any value of  $\mu$  and  $\Gamma_{L,R}$  according to  $v \sim \sqrt{\mu \Gamma_L}$  and  $W \sim \sqrt{\mu / \Gamma_L}$ , provided that the ratio  $\Gamma_R / \Gamma_L$  and  $\Gamma_W$  are kept the same.

The order of magnitude values of the front velocity and the front widths are  $10^7$  cm/s (in accordance with (18)) and  $10 \mu\text{m}$ , respectively (Fig.4). For lateral dimensions of the order of  $100 \mu\text{m}$ , the switching times are thus less than 1 ns. The front width exceeds both the thickness of the structure  $d \sim 50$  nm and the mean free path of the electron in the well which can be estimated as  $\ell_m \sim 0.1 \dots 1 \mu\text{m}$  for  $\mu = 10^5$  V/cms<sup>8</sup>. Hence the local approximation in (1) and the drift-diffusion approximation (3) for the lateral transport in the well are indeed justified for the obtained front solutions. Cold fronts are faster and wider than hot fronts. This is the result of the higher contrast between  $n_{on}$  and  $n_{off}$  near the right turning point  $u_{th}$  of the current-voltage characteristic. The estimate of Eqn. (18) for the same set of parameters is shown in Fig.4(a) by the dashed line. Despite of the rough approximations adopted to derive (18) (see Appendix), it gives the correct order of the magnitude of the front velocity.

In order to evaluate the significance of heating of the electron gas in the well we have performed simulations for  $T_W \sim E_e^F / k = 100$  K, which corresponds to the upper bound of the electron temperature  $T_W$  (Fig.4a, curve 2). It is found that heating has a visible but minor effect on front velocity. This indicates the drift-dominated lateral transport in the quantum well. To confirm this conclusion we have also performed simulations for  $T_W = 0$ , when lateral diffusion in the well is minimized and have found that the front velocity is practically the same as for  $T_W = T = 4$  K (Fig.4a, curve 1). Generally, according to (3) the drift component of the lateral current is much larger than the diffusion component for  $n \gg \rho_0 k T_W$ <sup>8</sup>. As it follows from the characteristic shown in Fig.2, for  $T = T_W$  this condition is satisfied for almost the whole range of concentrations  $[n_{on}, n_{off}]$  within the propagating front. Note that since the effective diffusion coefficient in (3) is concentration-dependent, the voltage  $u_{co}$  shifts with electron temperature  $T_W$ . The right and left extreme points for  $u_{co}$  correspond to the limits  $T_W \rightarrow 0$  (pure drift) and  $T_W \rightarrow \infty$  (pure diffusion), respectively.

## V. DISCUSSION: TOWARDS EXPERIMENTAL OBSERVATION OF FRONT DYNAMICS.

Since the pioneering work<sup>1</sup> the experimental observation of bistability in DBRT structures has become a routine. Despite of this, to the best of our knowledge lateral current density patterns in the DBRT, predicted already several years ago, have not yet been observed experimentally. Below we discuss the potential problems of such measurements in view of our theoretical findings.

*Sectional design of DBRT structure.* Achievements of modern growth technology have made it possible to manufacture resonant-tunneling structures with sophisticated design<sup>21,22</sup>, opening up the way to study transverse current density patterns in the DBRT experimentally. Here we propose the simplest design of a DBRT diode with a sectional emitter that allows to trigger a current density front and to observe its propagation by means of electrical measurements. Such a device constitutes of identical sections with individual emitters but common collector so that the bias can be applied separately to each section. To trigger a hot front the system should be prepared in the uniform off-state. This can be done by applying a voltage  $u > u_h$  to all emitter sections and subsequently decreasing this voltage to a value  $u_h < u < u_{co}$ . Then the DBRT can be switched on locally by a short negative voltage pulse  $u < u_h$ , applied to either lateral or central section of the device. The resulting front propagation can be monitored by measuring the electrical current in the parallel sections of the device.

*Barriers asymmetry.* Our results suggest that to achieve the widest bistability range the transparency of the well-collector barrier should be approximately 5 times smaller than the transparency of the emitter-well barrier.

*Front velocity and time resolution.* Our simulations show that the order of magnitude values of the front velocity and width are  $10^7$  cm/s and  $10 \mu\text{m}$ , respectively. It implies that the lateral dimension of suitable DBRT structure should exceed  $100 \mu\text{m}$ . Since it takes about 1 ns for the front to cross such a structure, reliable measurements of front propagation demand for time resolution of 100 ps or better. The fronts become slower with decreasing transparency of the barriers  $\Gamma_L$  and  $\Gamma_R$ . However, then the front width  $W$  will increase (see Eq.(19)), setting severe additional limitations on the lateral dimension of the appropriate DBRT structure. For example, decreasing  $\Gamma_{L,R}$  by one order of magnitude to the values  $\Gamma_L = 0.05$  meV,  $\Gamma_R = 0.01$  meV results in a front width of the order of  $\sim 30 \mu\text{m}$ , whereas the width of the cold front can exceed  $100 \mu\text{m}$ . Finally we note that in the regime of coherent tunneling the front velocity is expected to be of the order of the Fermi velocity  $v_f = \sqrt{2E_e^F/m^*}$ <sup>4</sup>. This yields  $\sim 10^8$  cm/s for  $E_e^F = 10$  meV.

*Hot or cold fronts ?* The width of a hot front is considerably smaller than the width of cold fronts and its velocity is somewhat lower (Fig.4). Hence a hot front is expected to be an easier target for experimental observation than a cold front.

*Pinning of the front.* Pinning on small imperfections of the reference media has been recognized as an important mechanism capable of preventing the front propagation in nonlinear systems<sup>23</sup>. In the case under consideration both technological imperfections of the DBRT structure and the spatial inhomogeneity due to the sectional DBRT design may play a role. Due to the exponential dependence of the barrier transparencies  $\Gamma_{L,R}$  on the barrier width, the embedded fluctuations of the barrier width are the most important among technological im-

perfections. In presence of imperfections the stationary current-voltage characteristic includes additional stable branches that correspond to nonuniform current density profiles associated with imperfections<sup>24</sup>. These steady non-uniform states remain observable, though the uniformly propagating fronts may not be possible in low-quality structures.

*Effect of the external circuit.* Generally, bistable DBRT elements can be operated via an external load. In contrast to the well known case of S-type bistability, in the system with Z-type bistability an external load provides a positive, not negative feedback upon front dynamics. In particular, stationary current density patterns are not stable even under current-controlled conditions<sup>7</sup>. An active external circuit which simulates a negative external load resistance and reverses the sign of feedback has been implemented experimentally in Ref. 2. We refer to Refs. 7, 25 for the further discussion of the effect of external circuit on dynamics and stability of current density patterns.

*DBRT-based 3-electrode switch.* The sectional DBRT with two small (control) sections separated by a large (main) section can be potentially used in applications as a controllable switch. By applying a control voltage pulse to the side sections, the rest of the structure can be switched to the on- or off-state via propagation of a lateral current density front. Note that in semiconductor device physics propagation of switching fronts in three-electrode bistable devices is a well known process which is used, e.g, in thyristors in certain regimes of operation<sup>26,27</sup>.

## ACKNOWLEDGMENTS

We are grateful to A. Wacker, L.E. Wernersson and V. Cheianov for useful discussions. This work has been supported by DFG in the framework of Sfb 555. One of the authors (P.R.) acknowledges support by the Alexander von Humboldt Foundation.

## APPENDIX: ANALYTICAL APPROXIMATION FOR THE FRONT VELOCITY.

In the limit  $\Gamma_W \ll E_F^e$  the local kinetic function becomes piecewise linear:

$$\begin{aligned}
 f(n, u) &= \frac{e\Gamma_L}{\hbar}(\lambda + \alpha_{RL} + 1) \left[ \frac{\rho_0(e\gamma u - E_W + E_e^F)}{\lambda + \alpha_{RL} + 1} - n \right] \\
 \text{for } n &\in \left[ \frac{\rho_0(e\gamma u - E_W)}{\lambda}, \frac{\rho_0(e\gamma u - E_W + E_e^F)}{\lambda} \right], \\
 f(n, u) &= -\frac{e\Gamma_L}{\hbar}\alpha_{RL}n \tag{A1} \\
 \text{for } n &\notin \left[ \frac{\rho_0(e\gamma u - E_W)}{\lambda}, \frac{\rho_0(e\gamma u - E_W + E_e^F)}{\lambda} \right],
 \end{aligned}$$

where the following notations have been introduced

$$\lambda \equiv \frac{4b_1b_2}{dr_B}, \quad \gamma \equiv \frac{b_1}{d}, \quad \alpha_{RL} \equiv \frac{\Gamma_R}{\Gamma_L}. \quad (\text{A2})$$

For a voltage  $u$  within the bistability range (note that  $u < 0$  and  $e < 0$ )

$$u_{th} = \frac{E_W}{e\gamma} + \frac{1}{e\gamma} \frac{\lambda E_e^F}{1 + \alpha_{RL}} < u < u_h = \frac{E_W}{e\gamma} \quad (\text{A3})$$

the electron concentration in the well is given by

$$\begin{aligned} n_{on} &= \frac{\rho_0(e\gamma u - E_W + E_e^F)}{\lambda + \alpha_{RL} + 1}; \\ n_{int} &= \frac{\rho_0(e\gamma u - E_W)}{\lambda}; \\ n_{off} &= 0 \end{aligned} \quad (\text{A4})$$

for on, intermediate and off states, respectively. The corresponding current-voltage characteristic is also piecewise linear.

Using (A1) and assuming for simplicity  $D(n) = D_0 = \text{const}$ , we find an explicit solution of Eqn.(13)

$$\begin{aligned} n(\xi) &= n_{int} \exp(\beta_1(v)\xi) \\ &\text{for } 0 < n < n_{int} \text{ and } -\infty < \xi < 0; \\ n(\xi) &= n_{on} - (n_{on} - n_{int}) \exp(-\beta_2(v)\xi) \\ &\text{for } n_{int} < n < n_{on} \text{ and } 0 < \xi < +\infty, \end{aligned} \quad (\text{A5})$$

where

$$\begin{aligned} \beta_1 &\equiv -\frac{v}{2D_0} + \sqrt{\left(\frac{v}{2D_0}\right)^2 + \frac{\Gamma_L}{\hbar D_0} \alpha_{RL}}; \\ \beta_2 &\equiv \frac{v}{2D_0} + \sqrt{\left(\frac{v}{2D_0}\right)^2 + \frac{\Gamma_L}{\hbar D_0} (\lambda + \alpha_{RL} + 1)}. \end{aligned} \quad (\text{A6})$$

Continuity of the first derivative  $dn/d\xi$  at  $\xi = 0$  gives the condition

$$(\beta_1(v) + \beta_2(v)) \frac{e\gamma u - E_w}{\lambda} = \beta_2(v) \frac{e\gamma u - E_w + E_e^F}{\lambda + \alpha_{RL} + 1}. \quad (\text{A7})$$

This condition (A7) implicitly determines the dependence of the front velocity  $v$  on the applied voltage  $u$ . Linearization of this dependence near the voltage

$$u_{co} = \frac{E_W}{e\gamma} + \frac{1}{e\gamma} \frac{\lambda E_e^F}{1 + \alpha_{RL} + \sqrt{\alpha_{RL}} \sqrt{\lambda + \alpha_{RL} + 1}} \quad (\text{A8})$$

that corresponds to  $v = 0$  leads to the explicit  $v(u)$ -dependence (15). The obtained dependence is equivalent to the linearization of Eqn.(14).

\* On leave from Ioffe Physicotechnical Institute, Politechnicheskaya 26, 194021, St.Petersburg, Russia. Electronic mail: rodin@physik.tu-berlin.de

- <sup>1</sup> V. J. Goldmann, D. C. Tsui and J. E. Cunningham, Phys. Rev. Lett. **58**, 1256 (1987).
- <sup>2</sup> A. Martin, M. Lerch, P. Simmonds and L. Eaves, Appl. Phys. Lett. **64**, 1248 (1994).
- <sup>3</sup> A. Wacker and E. Schöll, J. Appl. Phys. **78**, 7352 (1995).
- <sup>4</sup> B. Glavin, V. Kochelap and V. Mitin, Phys. Rev. B **56** 13346 (1997).
- <sup>5</sup> D. Mel'nikov and A. Podlivaev, Semiconductors **32**, 206 (1998).
- <sup>6</sup> M. N. Feiginov and V. A. Volkov, JETP Lett. **68**, 633 (1998) [Pis'ma Zh. Eksp. Teor. Fiz. **68**, 628 (1998)].
- <sup>7</sup> M. Meixner, P. Rodin, E. Schöll and A. Wacker, Eur. Phys. J B **13**, 157 (2000).
- <sup>8</sup> V. Cheianov, P. Rodin and E. Schöll, Phys. Rev. B **62**, 9966 (2000).
- <sup>9</sup> E. Schöll, A. Amann, M. Rudolf and J. Unkelbach, Physica B **314**, 113 (2002).
- <sup>10</sup> The expression for  $J_{ew}$  derived in Ref. 9 agrees with (4) for  $\Delta \gg kT_W, \Gamma_W$ . The expression for  $J_{ew}$  derived in Ref. 7 also includes an additional logarithmic term which gives a contribution of about 5 % for the chosen parameters. This term is skipped here for simplicity.
- <sup>11</sup> J. Inkoferer, G. Obermair and F. Claro, Phys. Rev. B **64**, 201404 (2001).
- <sup>12</sup> S. Datta, *Electronic Transport in Mesoscopic Systems*, (Cambridge University Press, Cambridge 1995)
- <sup>13</sup> The spacer layer in the emitter is not taken into account here.
- <sup>14</sup> P. J. Price, *Electron Tunneling in Semiconductors*, in *Handbook on Semiconductors*, (edited by P. T. Landsberg), Vol.1 (Elsevier, Amsterdam 1992).
- <sup>15</sup> P. Guèret, C. Rossel, E. Marclay, and H. Meier, J. Appl. Phys. **66**, 278 (1989).
- <sup>16</sup> B. K. Ridley, *Electrons and Phonons in Semiconductor Multilayers*, (Cambridge University Press, Cambridge 1995), p.23, eqn.(1.29).
- <sup>17</sup> V. Karpus, Semicond. Sci. Technol. **5**, 691 (1990).
- <sup>18</sup> Note that at  $T = 4$  K the momentum and energy relaxation times in the quantum well are determined by interface roughness scattering and acoustic phonon scattering, respectively <sup>16,17</sup>.
- <sup>19</sup> The monotonic dependence of the bistability range on the dimensionless parameter  $k = \Gamma_L/(\Gamma_L + \Gamma_R)$  has also been reported in Ref. 4 for the coherent tunneling model.
- <sup>20</sup> E. Schöll, *Nonlinear Spatio-Temporal Dynamics and Chaos in Semiconductors* (Cambridge University Press, 2001).
- <sup>21</sup> L.-E. Wernersson, M. Suhara, N. Carlsson, K. Furuya, B. Gustafson, A. Litwin, L. Samuelson, and W. Seifert, Appl. Phys. Lett. **74**, 311 (1999).
- <sup>22</sup> L.-E. Wernersson, M. Borgström, B. Gustafson, A. Gustafsson, L. Jarlskog, J.-O. Malm, A. Litwin, L. Samuelson, and W. Seifert, J. Crystal Growth **221**, 704 (2000).
- <sup>23</sup> I. Mitkov, K. Kladko and J. E. Pearson, Phys. Rev. Lett. **81**, 5453 (1998)

- <sup>24</sup> A. M. Nechaev, B. F. Sinkevich, *Sov. Phys. Semicond.*, **18**, 218 (1984) [*Fiz. Tekh. Polupr.* **18**, 350 (1984)].  
<sup>25</sup> A. Alekseev, S. Bose, P. Rodin and E. Schöll, *Phys. Rev. E* **57**, 2640 (1998).

- <sup>26</sup> S. M. Sze, *Modern Semiconductor Device Physics*, (Wiley, New York, 1998).  
<sup>27</sup> M. Meixner, P. Rodin and E. Schöll, *Phys. Rev. E* **58**, 2796 (1998).

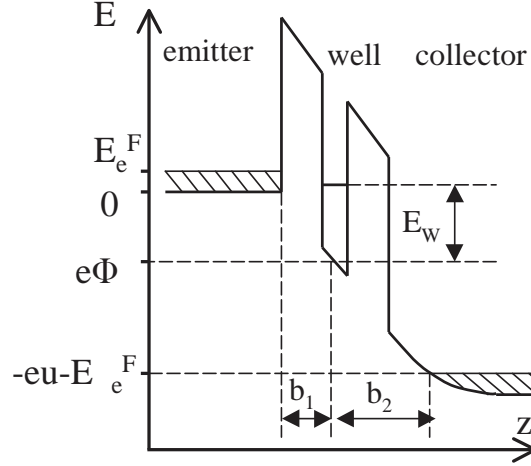


FIG. 1. Schematic DBRT structure. Note that the applied voltage  $u$  and the electron charge  $e$  are chosen negative.

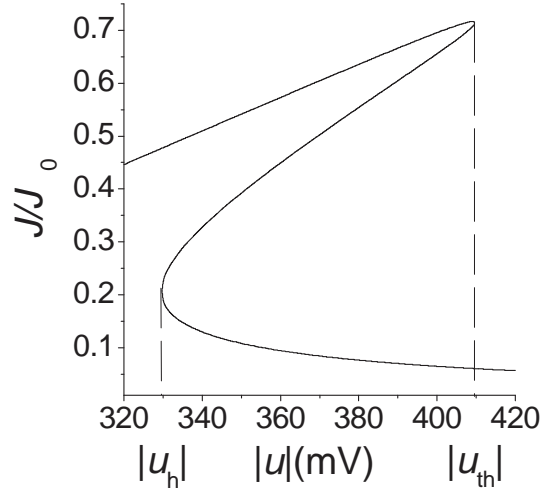


FIG. 2. Stationary current-voltage characteristic of the DBRT in the bistable regime. The current density  $J$  is normalized by  $J_0 = e\Gamma_R\rho_0E_e^F/\hbar$ . This normalized current density is equivalent to the normalized electron concentration in the well:  $J/J_0 \equiv n/(\rho_0E_e^F)$ . The corresponding numerical values are  $J_0 \approx 7 \text{ kA/cm}^2$  and  $\rho_0E_e^F \approx 3 \cdot 10^{11} \text{ cm}^{-2}$  for the chosen parameters  $E_e^F = 10 \text{ meV}$ ,  $b_1 = 10 \text{ nm}$ ,  $b_2 = 50 \text{ nm}$ ,  $\Gamma_L = 0.5 \text{ meV}$ ,  $\Gamma_R = 0.1 \text{ meV}$  and  $\Gamma_W = 2.0 \text{ meV}$ .

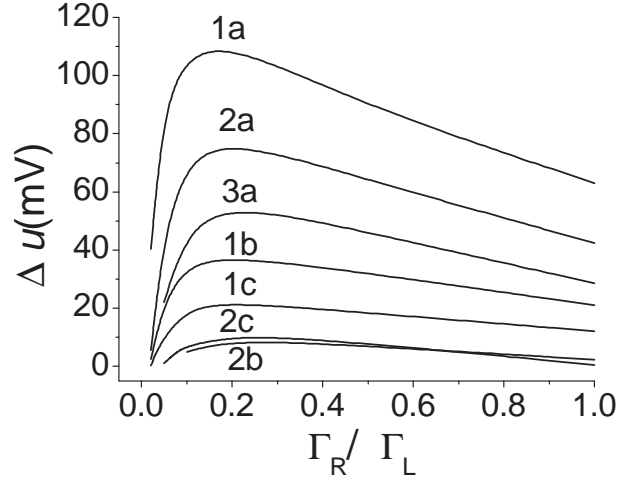


FIG. 3. Bistability range as a function of  $\Gamma_R/\Gamma_L$ . Parameters:  $E_e^F = 10$  meV,  $b_1 = 10$  nm,  $b_2 = 50$  nm and  $\Gamma_W = 1$  meV, 2 meV, 3 meV for curves 1a, 2a, 3a, respectively;  $E_e^F = 5$  meV,  $b_1 = 10$  nm,  $b_2 = 50$  nm and  $\Gamma_W = 1$  meV, 3 meV for curves 1b, 2b, respectively;  $E_e^F = 5$  meV,  $b_1 = 10$  nm,  $b_2 = 30$  nm and  $\Gamma_W = 1$  meV, 3 meV for curves 1c and 2c, respectively.

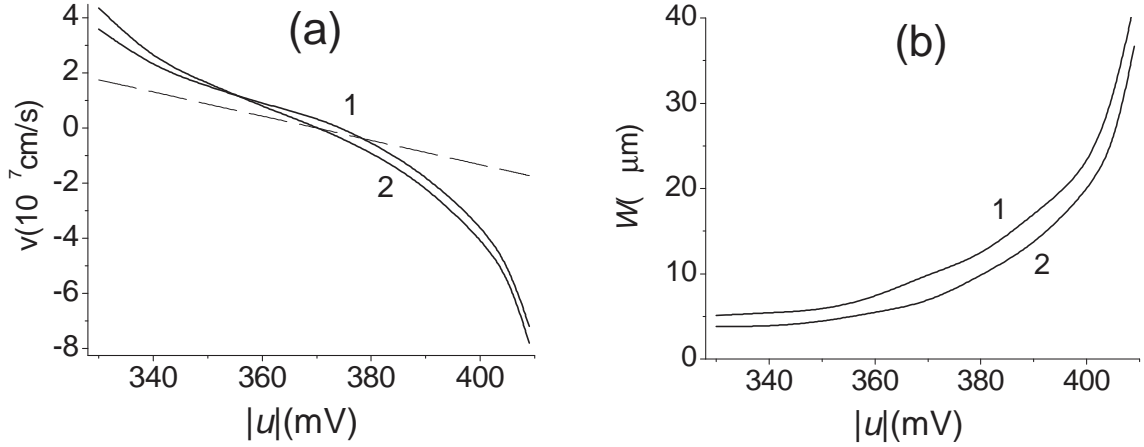


FIG. 4. Front velocity (a) and front width (b) as a function of the applied voltage  $u$ . Curves 1 and 2 correspond to  $T_W = 4K$  and  $T_W = 100K$ , respectively. The dashed line in the panel (a) shows the prediction of the analytical formula (18) with  $u_{co}$  approximated as  $u_{co} = (u_{th} + u_h)/2$ . Parameters as in Fig.2 :  $\Gamma_L = 0.5$  meV,  $\Gamma_R = 0.1$  meV,  $\mu = 10^5$  cm<sup>2</sup>/V · s.